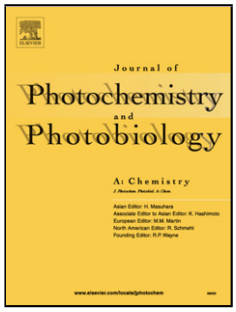

Title: Photo-control of cancer cell growth by benzodiazo *N*-substituted pyrrole derivatives

Authors: Concetta Imperatore, Maria Scuotto, Mohammadhassan Valadan, Elisa Rivieccio, Assunta Saide, Annapina Russo, Carlo Altucci, Marialuisa Menna, Anna Ramunno, Luciano Mayol, Giulia Russo, Michela Varra

PII: S1010-6030(18)31776-3
DOI: https://doi.org/10.1016/j.jphotochem.2019.03.042
Reference: JPC 11779

To appear in: *Journal of Photochemistry and Photobiology A: Chemistry*

Received date: 5 December 2018
Revised date: 19 March 2019
Accepted date: 25 March 2019

Please cite this article as: Imperatore C, Scuotto M, Valadan M, Rivieccio E, Saide A, Russo A, Altucci C, Menna M, Ramunno A, Mayol L, Russo G, Varra M, Photo-control of cancer cell growth by benzodiazo *N*-substituted pyrrole derivatives, *Journal of Photochemistry and amp; Photobiology, A: Chemistry* (2019), https://doi.org/10.1016/j.jphotochem.2019.03.042

Photo-control of cancer cell growth by benzodiazo *N*-substituted pyrrole derivatives

Concetta Imperatore[†a], Maria Scuotto[†a], Mohammadhassan Valadan[b], Elisa Rivieccio[a], Assunta Saide[a], Annapina Russo[a], Carlo Altucci[b], Marialuisa Menna[a], Anna Ramunno[c], Luciano Mayol[a], Giulia Russo*[a] and Michela Varra*[a]

[a] *Department of Pharmacy, University of Naples Federico II, Naples 80131, Italy. e-mail varra@unina.it; correspondence can be also sent to giulia.russo@unina.it.*
[b] *Department of Physics "Ettore Pancini", University of Naples Federico II, Naples 80126, Italy.*
[c] *Department of Pharmacy/DIFARMA, University of Salerno, 84084 Fisciano, Salerno, Italy.*
[†]*These authors contributed equally to the manuscript.*

Graphical abstract

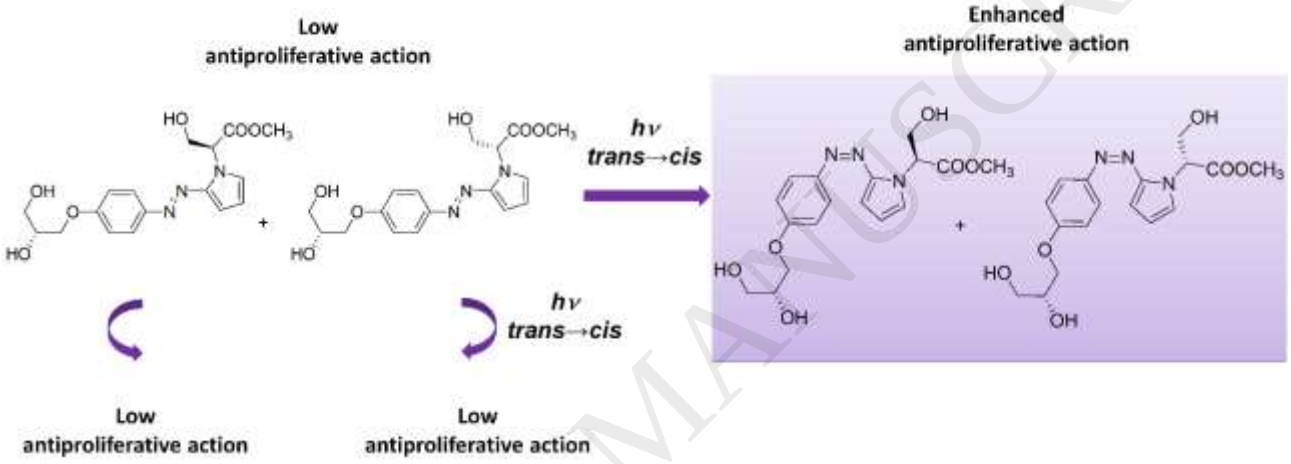

highlights

- The new reported compounds easily switch from the *trans* to the *cis* form after LED irradiation;
- the UV spectra reveal the reversibility of *trans*↔*cis* isomerisation;
- after irradiation the *trans-cis* photo-conversions are detectable in ^{1}H NMR spectra;
- kinetics of the *trans*↔*cis* isomerisations were evaluated by UV and fast UV experiments;
- the compounds differently affect the dynamic of MT polymerization after UV irradiation;
- under irradiation the compounds affect HCT-116 p53-/- cell viability.

Abstract

In order to expand the class of diazocompounds able to act as photo-activable microtubule inhibitors the potential of azo-heteroarenes has been explored. In this paper we focus on the synthesis, physical properties and biological effects of methyl *rac*-2-(2-((*E*)-(4-((*R*)-2,3-dihydroxypropoxy)phenyl) diazenyl)-1H-pyrrol-1-*yl*)-3-hydroxypropanoate (**1a**) and methyl *rac*-2-(2-((*E*)-(4-((*S*)-2,3-dihydroxypropoxy)phenyl) diazenyl)-1H-pyrrol-1-*yl*)-3-hydroxypropanoate (**1b**). Preliminary biological studies on the HCT-116 p53-/- cancer cell line have shown that the weak antiproliferative action of the *trans* isomers of these molecules, especially of **1a,** is enhanced upon

LED light irradiation at 435 nm. On A375 cells the molecules have not shown any effect on cell viability either in the dark or under irradiation. Moreover, the two diastereomeric components of **1a** as pure stereomers have been synthesized and characterized for their chemical-physical properties. Interestingly, upon irradiation, **1a** has shown an antiproliferative activity on the HCT-116 p53-/- cells greater than that of the pure stereomers, 1**RR** and 1**RS**. Tubulin polymerization assay has also demonstrated that **1a**, **1RR** and **1RS** inhibit tubulin aggregation mostly after exposure of the samples to LED light irradiation.

key words: *N*-substituted pyrrole, diazocompounds, tubulin inhibitors.

1. Introduction

Targeting a remote, non-invasive, spatiotemporal control of specific biological systems through light induced *stimuli* has gained increasing attention in recent years [1-5]. Nowadays, the term *photopharmacology* refers to these therapeutic approaches, in which the key role is played by photo-responsive molecules or molecular portion(s), that, switching to different molecular states upon specific irradiation, undergo changes in their pharmacokinetic or pharmacodynamic properties [1-3].

Azobenzenes (AzBs) are one of the most interesting classes of photo-responsive molecules because of their quantitative and reversible, light induced, *trans-cis* photoisomerization [4,5]. The control of some ionotropic glutamate receptors [6,7], the folding-unfolding of the three-dimensional structure of peptides [8] or nucleic acids [9], and the building of photosensitive supra-molecular architectures [10], represent only a few examples of the potential applications of photo-switchable AzBs.

Interestingly, the *cis* isomers of some AzBs, named photostatins (PSTs, Figure 1), are potential tools for anti-cancer therapy in view of their ability to target microtubules [11-13] (MTs). MTs are dynamic structures involved in the control of a great number of cellular events, including cell signalling, cell division and mitosis [14]. Since cancer cells proliferate rapidly and uncontrollably, MTs represent an attractive target in cancer therapy. However, since MTs are key components of the cytoskeleton common to all eukaryotic cells, almost all microtubule targeting agents (MTAs) are highly toxic. PSTs are analogues of combretastatin A-4 (CA4), a natural ligand of MTs; they were designed by changing the exocyclic C=C into a N=N bond (Figure 1). The affinities of PSTs towards the MT colchicine binding site were turned on by irradiation of their stable *trans* isomers into the corresponding *cis* isomers. Thus, a local and specific activation through irradiation prevents the side effects associated with the perturbation of the MT dynamics in normal cells, revealing PSTs as new efficient MTAs [15-17]. Despite this, only a few examples of AzB analogues as potential photo-activable MTAs have been reported until now [11-13,18]. In accordance with their distinctive properties, the exploration of different typologies of AzBs is advisable.

Moreover, several CA4 analogues have been discovered in the last few years [17,19-21], modified at the phenyl rings and/or at the double carbon bond. In particular, the replacement of the exocyclic C=C with a heterocyclic aromatic moiety (i.e. pyrroles, imidazoles, thiazoles, thiophenes, etc,) [19] not only allowed the desired *cis-like* conformational constraint but also introduced new pharmacological properties, because of the incorporation of heteroatoms. It is noteworthy that the etheroarene diazo derivatives show interesting optical properties, compared to those of the unsubstituted AzBs [22-24]. Indeed, they switch from the *trans* to the *cis* form by irradiation with low intensity light having red-shifted wavelengths, thus limiting the disadvantages of any possible radiation treatment. In fact, it is known that radiation having a wavelength not significantly down-shifted towards the UV side of the light spectrum (typically $\lambda \geq 400$ nm) and intensities not exceeding ≈ 10 mW/cm^2, does not trigger any undesired damaging processes in the treated live

matter. Typically, such damaging processes occur with λ < 400 nm and/or higher intensities [25 and references therein for a general presentation of the interaction mechanisms and triggered processes between IR-Visible-UV radiation and live matter].

Furthermore, the regioselectivity at Cα of the pyrrole, that is retained in *N*-substituted pyrrole derivatives, increases the yields of coupling in reactions with azonium salts, also enlarging the pool of *N*-substituted diazo compounds to be investigated [17].

In order to explore the potential of diazo-heteroarenes as cancer cell growth inhibitors, we synthesized methyl *rac*-2-(2-((*E*)-(4-((*R*)-2,3-dihydroxypropoxy)phenyl)diazenyl)-1H-pyrrol-1-*yl*)-3-hydroxypropanoate **1a** and methyl *rac*-2-(2-((*E*)-(4-((*S*)-2,3-dihydroxypropoxy)phenyl)diazenyl)-1H-pyrrol-1-*yl*)-3-hydroxypropanoate **1b** (Figure 1 and Scheme 1). The solvated samples **1a** and **1b** were then subjected to in depth investigation to characterize their physical and biological properties. In view of the increasing of the antiproliferative effect of **1a** on the viability of the HCT-116 p53-/- cells under irradiation compared to the darkness regimen, its pure stereomers **1RR** and **1RS** were also synthesized and tested (Scheme 1). The photo-activated **1RR** and **1RS** as well as their effects on cancer cells were evaluated. In order to preliminarily investigate the mechanism of action of **1a** and of its pure components, a light-scattering-based tubulin polymerization assay was run under both dark and irradiation conditions.

2. MATERIAL AND METHODS

2.1. General

Chemicals and anhydrous solvents were purchased from Sigma-Aldrich. TLCs were run on Merck silica gel 60 F254 plates and the spots were visualized by means of an UV lamp (Vilber Lourmat VL-4LC, 365 and 254 nm). Silica gel chromatography was performed using Merck silica gel 60 (0.063–0.200 mm). HPLC purifications and analyses were carried out using a JASCO PU-2089 Plus HPLC pump equipped with a JASCO BS-997-01 UV detector. CD experiments were performed on a JASCO 715 spectropolarimeter equipped with a PTC-348 temperature controller. UV experiments were performed on a JASCO V-530 spectrophotometer, equipped with a PTC-348 temperature controller. HRESIMS (high resolution electrospray ionization mass spectrometry) analyses were performed on a Thermo LTQ Orbitrap XL mass spectrometer (Thermo-Fisher, San Josè, CA, USA). The spectra were recorded by infusion into the ESI (Thermo-Fisher, San Josè, CA, USA) source using MeOH as solvent. The [α] values were measured with JASCO polarimeter P-2000. ^{1}H (500 MHz and 400 MHz) and ^{13}C (125 MHz) NMR spectra were recorded on an Agilent INOVA spectrometers (Agilent Technology, Cernusco sul Naviglio, Italy); chemical shifts were referenced to the residual solvent signal (CD_3OD: δ_H = 3.31, δ_C = 49.0 ppm; C_6D_5N: δ_H = 7.19, 7.55 and 8.71 ppm). For an accurate measurement of the coupling constants, the one-dimensional ^{1}H NMR spectra were transformed at 64 K points (digital resolution: 0.09 Hz). ^{1}H connectivities were determined by COSY and TOCSY experiments (mixing time 100 ms). Through-space ^{1}H connectivities were evidenced using a ROESY experiment with a mixing time of 500 ms. Two and three bond ^{1}H-^{13}C connectivities were determined by gradient 2D HSQC experiments optimized for a $^{2,3}J$ of 8 Hz. $^{3}J_{H\text{-}H}$ values were extracted from 1D ^{1}H NMR.

2.2. Synthesis

***R* or *S* 3-(4-nitrophenoxy)propane-1,2-diol (2R/2S)**. A mixture of 4-nitrophenol, (0.500 g, 3.6 mmol), KOH (1.0 mg, 1.8x10^{-2} mmol, dissolved in 50 µL of EtOH) and dry toluene (2 mL) was stirred under reflux in a double neck flask. After 30 min, the mixture was cooled to r.t. and 287 µL of *R* or *S* glycidol (0.320 g, 4.3 mmol) were slowly added by a syringe. The mixture was further stirred at 90 °C for 24 h. The solvent was then evaporated under *vacuo* and the residue dissolved in MeOH. The obtained solution was embedded on silica and then evaporated to dryness. The resulting

powder was applied on a ethyl acetate:acetone 70:30 (v/v) packed silica gel column eluted using isocratic conditions. The fractions containing the desired product were dried under *vacuo* to give *R* or *S* stereomer of **2** as a yellow gel (yields 85% and 86%, respectively). TLC plate R_f= 0.73 (ethyl acetate:acetone 70:30 (v/v)).

^{1}H NMR (CD_3OD) δ_H: 3.64–3.73 (m, 2H, CH_2OH), 3.97-4.05 (m, 1H, CHOH), 4.09 (dd, *J* = 6.1, 9.8 Hz, 1H, OCH_2), 4.18 (dd, *J* = 4.1, 9.8 Hz, 1H, OCH_2), 7.05–7.10 (m, 2H, $C^{2,6}_{Ar}H$), 8.14–8.20 (m, 2H, $C^{3,5}_{Ar}H$). ^{13}C NMR (CD_3OD) δ_C: 63.9 (CH_2OH), 71.2 (CHO), 71.4 (CH_2O), 115.8 ($C^{2,6}_{Ar}$), 126.8 ($C^{3,5}_{Ar}$), 142.8 (C^4_{Ar}), 165.5 (C^1_{Ar}). HRESIMS (positive ion mode, CH_3OH) m/z 236.0533 $[M+Na]^+$ (calcd for $C_9H_{11}NO_5Na$, 236.0529).

$[\alpha]_{25}$ *R*= -17.8 [c= 12.4 mg/mL; EtOH] *S*=+16.9 [c= 19.2 mg/mL; EtOH].

***R* or *S* 3-(4-aminophenoxy)propane-1,2-diol (3R/3S)**. A mixture of **2** (*R* or *S*, 0. 560 g, 2.6 mmol), Pd/C (5% w/w, 28 mg) and 25 mL EtOH (90%, HPLC grade) was stirred in a Parr apparatus under hydrogen atmosphere (P= 400 psi). After 1.5-2.0 h the reaction was monitored by disappearance of UV spot of **2** on TLC plate (R_f= 0.73, ethyl acetate:acetone 70:30 (v/v) and the appearance of a new UV spot strongly sensitive to ninhydrin (R_f= 0.46). The mixture was filtered, and the eluted solution dried in *vacuo*, to obtain **3R** or **3S** as brick-red solid, that was further purified by crystallization from DCM:MeOH 7:3 (0.440 g, yields 93%).

^{1}H NMR (CD_3OD) δ_H: 3.62 (dd, *J* = 5.4, 11.2 Hz, 1H, CH_2OH), 3.67 (dd, *J* = 4.8, 11.2 Hz, 1H, CH_2OH), 3.89–3.84 (m, 1H, CHOH), 3.91 (dd, *J* = 5.1, 9.8 Hz, 1H, OCH_2), 3.95 (dd, *J* = 4.1, 9.8 Hz, 1H, OCH_2), 6.70 (d, *J* = 8.8 Hz, 2H, $C^{2,6}_{Ar}H$), 6.76 (d, *J* = 8.8 Hz, 2H, $C^{3,5}_{Ar}H$). ^{13}C NMR (CD_3OD) δ_C: 64.3 (CH_2OH), 71.1 (CHO), 71.9 (CH_2O), 118.1 ($C^{2,6}_{Ar}$), 116.6 ($C^{3,5}_{Ar}$), 141.8 (C^4_{Ar}), 153.6 (C^1_{Ar}). HRESIMS (positive ion mode, CH_3OH) m/z 184.0980 $[M+H]^+$ (calcd for $C_9H_{14}NO_3$, 184.0974).

1a, **1b**, **1RR** and **1RS**. A mixture of **3R** or **3S** (0.400 g, 2.2 mmol), 205 µL fluoroboric acid (water solution, 48% v/v, 3.3 mmol) 4 mL of EtOH was cooled to -15 °C under argon and then 224 µL of isoamyl nitrite (0.258 g, 2.2 mmol) were added. After 12 h under stirring, the produced diazonium salt was first precipitated diluting the mixture with *n*-hexane, and then further washed with *n*-hexane (three times). The solid residue was dried under *vacuo* to give **4R** or **4S**, which was used in the next step without further treatment. The intermediate **4R** or **4S** (0.360 g, 1.8 mmol) was dissolved in 10 mL of acetic acid (14 g, 232 mmol), under stirring. Sodium acetate (4.0 g, 511 mmol) and ***rac*-5** or **5R** or **5S** (254 µL, 0.270 g, 2.2 mmol) were added, consecutively, to the solution [26]. After 15 min at r.t., the formation of a gel-like mixture was observed. The reaction time was further prolonged up to 1 h, under slow stirring. The final mixture was diluted with water and extracted with DCM (4-5 times). The collected organic layers were dried under *vacuo* and the residue dissolved in MeOH. The obtained solution was embedded on silica and then evaporated to dryness. The resulting powder was applied on a DCM:propan-2-ol 90:10 (v/v) packed silica gel column and then chromatographed using isocratic conditions. The collected fractions, dried under *vacuo* (TLC 90:10 DCM:MeOH, v/v, R_f= 0.6) were further purified on HPLC RP-18 column (H_2O:ACN, 80:20, v/v, t_R= 12 min), to get 0.185 of **1b** (yields 51%), 0.210 g of **1a** (yields 58%), 0.214 g of **1RR** or **1RS** (yields 59%). NMR spectra of each species are all reported in the SI.

1a. ^{1}H NMR (CD_3OD) δ_H: 3.66 (m, 2H, CH_2OH), 3.67 (s, 3H, OCH_3), 3.99 (m, 1H, CHOH), 4.13 (dd, *J* = 4.2, 9.6 Hz, 1H, OCH_2),), 4.19 (dd, *J* = 6.8, 11.7 Hz, 1H, CH_2OH), 4.24 (dd, *J* = 4.7, 11.7 Hz, 1H, CH_2OH pyrrole 4.24 (dd, *J* = 6.0, 9.6 Hz, 1H, OCH_2), 5.62 (dd, *J* = 4.8, 6.6 Hz, 1H, $CHCOCH_3$), 6.32 (dd, *J* = 3.0, 3.38 Hz, 1H, C^4_{pyrr}), 6.67 (dd, *J* = 1.2, 3.9 Hz, 1H, C^3_{pyrr}), 7.04 (d, *J* = 8.9 Hz, 2H, $C^{2,6}_{Ar}H$), 7.28 (~~s,~~ m, 1H, C^5_{pyrr}), 7.70 (d, *J* = 8.9 Hz, 2H, $C^{3,5}_{Ar}H$). ^{13}C NMR (CD_3OD) δ_C: 51.8 (OCH_3), 60.2 ($CHCOCH_3$), 62.8 (CH_2OH), 70.5 (CHOH), 69.5 (OCH_2), 69.4 (CH_2OH), 99.9 (C^3_{pyrr}), 110.0 (C^4_{pyrr}), 126.2 (C^5_{pyrr}), 147.8 (C^2_{pyrr}), 114.7 ($C^{2,6}_{Ar}$), 123.4 ($C^{3,5}_{Ar}$), 145.5 (C^4_{Ar}), 160.7 (C^1_{Ar}), 170.2 ($COCH_3$).

1b. ^{1}H NMR (CD_3OD) δ_H: 3.66 (m, 2H, CH_2OH), 3.67 (s, 3H, OCH_3), 3.99 (m, 1H, CHOH), 4.13 (dd, *J* = 4.2, 9.6 Hz, 1H, OCH_2),), 4.19 (dd, *J* = 6.8, 11.7 Hz, 1H, CH_2OH), 4.24 (dd, *J* = 4.7, 11.7 Hz, 1H,

CH_2OH pyrrole 4.24 (dd, *J* = 6.0, 9.6 Hz, 1H, OCH_2), 5.62 (dd, *J* = 4.8, 6.6 Hz, 1H, $CHCOCH_3$), 6.32 (dd, *J* = 3.0, 3.38 Hz, 1H, C^4_{pyrr}), 6.67 (dd, *J* = 1.2, 3.9 Hz, 1H, C^3_{pyrr}), 7.04 (d, *J* = 8.9 Hz, 2H, $C^{2,6}_{Ar}H$), 7.29 (~~s~~m, 1H, C^5_{pyrr}), 7.70 (d, *J* = 8.9 Hz, 2H, $C^{3,5}_{Ar}H$). ^{13}C NMR (CD_3OD) δ_C: 51.8 (OCH_3), 60.2 ($CHCOCH_3$), 62.8 (CH_2OH), 70.5 (CHOH), 69.5 (OCH_2), 69.4 (CH_2OH), 99.9 (C^3_{pyrr}), 110.0 (C^4_{pyrr}), 126.2 (C^5_{pyrr}), 147.8 (C^2_{pyrr}), 114.7 ($C^{2,6}_{Ar}$), 123.4 ($C^{3,5}_{Ar}$), 145.5 (C^4_{Ar}), 160.7 (C^1_{Ar}), 170.2 ($COCH_3$).

1RR. ^1H NMR (CD_3OD) δ_H: 3.66 (m, 2H, CH_2OH), 3.67 (s, 3H, OCH_3), 3.99 (m, 1H, CHOH), 4.13 (dd, *J* = 4.2, 9.6 Hz, 1H, OCH_2),), 4.19 (dd, *J* = 6.8, 11.7 Hz, 1H, CH_2OH), 4.24 (dd, *J* = 4.7, 11.7 Hz, 1H, CH_2OH pyrrole 4.24 (dd, *J* = 6.0, 9.6 Hz, 1H, OCH_2), 5.62 (dd, *J* = 4.8, 6.6 Hz, 1H, $CHCOCH_3$), 6.32 (dd, *J* = 3.0, 3.38 Hz, 1H, C^4_{pyrr}), 6.67 (dd, *J* = 1.2, 3.9 Hz, 1H, C^3_{pyrr}), 7.04 (d, *J* = 8.9 Hz, 2H, $C^{2,6}_{Ar}H$), 7.29 (~~s~~m, 1H, C^5_{pyrr}), 7.70 (d, *J* = 8.9 Hz, 2H, $C^{3,5}_{Ar}H$). ^{13}C NMR (CD_3OD) δ_C: 51.8 (OCH_3), 60.2 ($CHCOCH_3$), 62.8 (CH_2OH), 70.5 (CHOH), 69.5 (OCH_2), 69.4 (CH_2OH), 99.9 (C^3_{pyrr}), 110.0 (C^4_{pyrr}), 126.2 (C^5_{pyrr}), 147.8 (C^2_{pyrr}), 114.7 ($C^{2,6}_{Ar}$), 123.4 ($C^{3,5}_{Ar}$), 145.5 (C^4_{Ar}), 160.7 (C^1_{Ar}), 170.2 ($COCH_3$).

1RS. ^1H NMR (CD_3OD) δ_H: 3.66 (m, 2H, CH_2OH), 3.67 (s, 3H, OCH_3), 3.99 (m, 1H, CHOH), 4.13 (dd, *J* = 4.2, 9.6 Hz, 1H, OCH_2),), 4.19 (dd, *J* = 6.8, 11.7 Hz, 1H, CH_2OH), 4.24 (dd, *J* = 4.7, 11.7 Hz, 1H, CH_2OH pyrrole 4.24 (dd, *J* = 6.0, 9.6 Hz, 1H, OCH_2), 5.62 (dd, *J* = 4.8, 6.6 Hz, 1H, $CHCOCH_3$), 6.32 (dd, *J* = 3.0, 3.38 Hz, 1H, C^4_{pyrr}), 6.67 (dd, *J* = 1.2, 3.9 Hz, 1H, C^3_{pyrr}), 7.04 (d, *J* = 8.9 Hz, 2H, $C^{2,6}_{Ar}H$), 7.29 (~~s~~m, 1H, C^5_{pyrr}), 7.70 (d, *J* = 8.9 Hz, 2H, $C^{3,5}_{Ar}H$). ^{13}C NMR (CD_3OD) δ_C: 51.8 (OCH_3), 60.2 ($CHCOCH_3$), 62.8 (CH_2OH), 70.5 (CHOH), 69.5 (OCH_2), 69.4 (CH_2OH), 99.9 (C^3_{pyrr}), 110.0 (C^4_{pyrr}), 126.2 (C^5_{pyrr}), 147.8 (C^2_{pyrr}), 114.7 ($C^{2,6}_{Ar}$), 123.4 ($C^{3,5}_{Ar}$), 145.5 (C^4_{Ar}), 160.7 (C^1_{Ar}), 170.2 ($COCH_3$).

ε (CH_3OH)= $1.05x10^4$ $M^{-1}cm^{-1}$; ε(PBS)= $1.00x10^4$ $M^{-1}cm^{-1}$.

HRESIMS (positive ion mode, CH_3OH) **1a** m/z 364.1510 $[M+H]^+$; **1b** m/z 364.1498 $[M+H]^+$; **1RR** m/z 364.1506 $[M+H]^+$; **1RS** m/z 364.1506 $[M+H]^+$ (calcd for $C_{17}H_{22}N_3O_6$, 364.1503). $[\alpha]_{25}$ **1RR** = +12.0 [c= 26.6 mg/mL; MeOH] **1RS** = -12.6 [c= 29.3 mg/mL; MeOH].

2.3. Chiral HPLC

2, as *R* or *S* stereomer and a mixture of both species were analyzed on ChiralpaK 1A column (4.6x250 mm, particle size: 5micron, Figure S1) eluted with 90:10 *n*-hexane:propan-2-ol. t_R = 33.85 min for *R*-3-(4-nitrophenoxy)propane-1,2-diol; t_R = 38.55 min for *S*-3-(4-nitrophenoxy)propane-1,2-diol. **1RR**, **1RS** and **1a** were analyzed on cellulose-3 chiral column (4.6x100 mm, particle size: 3 micron, Figure S2) eluted with 80:20 *n*-hexane:propan-2-ol. t_R of **1RR** was 13.4 min and that of **1RS** was 19.8 min. **1RR** and **1RS** differed in their CD profiles, both showing a Cotton effect centred at about 400 nm but having almost opposite signature (Figure S3).

2.4. UV spectroscopy

In order to obtain data related to the *trans* isomer, the cuvette (0.1 o.l. Vol. 400 µL) containing 40 or 80 µM of **1a** or **1b** in MeOH was taken in dark at r.t. for about 12 h. UV spectra of the *cis* isomers were acquired after irradiation of the samples at 400, 435 or 505 nm (1 min, 1 LED 400, 435, or 505 nm Roithner Lasertechnik [11]). The *cis* thermal decay was monitored by further sequential acquisition of spectra (every two minutes) until the UV profile became that of the initial *trans* isomer. In order to obtain the $t_{1/2}$ of *cis* isomer, after the sample irradiation at 435 nm, UV time course measurement experiments were performed monitoring the absorbance values at 340, 390, 400, 425, and 505 nm, number of cycle 100-180, cycle time 60 s. The spectra showing the *cis*→*trans* photo-conversion were obtained after irradiation with green light (1 min, 1 LED 505 nm). Samples for UV experiments in PBS were prepared mixing 63 or 126 µL of **1a** or **1b** (1.0 mM in DMSO) and 1400 µL of PBS. Finally, the stability of **1a** or **1b** under the used light conditions, were verified acquiring spectra after 24 h of irradiation using the same pulse-program employed for biological assay. In particular, the UV cuvette containing **1a** or **1b** at 40 µM was exposed to pulsed LED at 435 or 505 nm. LEDs were managed by an Arduino module (50 ms-ON/ 1.0 min-OFF, 50 ms ON/1.0 s OFF; 50 ms ON /500 ms OFF; 500 ms ON/7.5 min OFF).

2.5. Fast UV spectroscopy

Samples were prepared by dissolving **1a** and **1b** molecules in different solvents: methanol, H_2O, and PBS. **6a** and **6b** were produced as a result of hydrolysis of the **1a/b** in water-based solutions. 2.0 mL of the sample was hold in a quartz cuvette, stirred by a magnetic stirrer, and transmission percentage at 404 nm in 10 mm optical path was monitored. A sketch of the optical setup for this experiment is shown in scheme S1.

2.6. Cell cultures and treatments

The HCT-116 p53 -/- [27] and A375 cell lines were cultured in Dulbecco's Modified Eagle's Medium (DMEM), supplemented with 10% fetal bovine serum (FBS) (Euroclone S.p.A), 2 mM L-glutamine and 50 U/ml penicillin-streptomycin, under humidified atmosphere of 5% CO_2 at 37 °C. Treatments of cells were performed replacing the culture medium with those containing indicated compounds at final concentration of 1 and 10 µM per well and exposed or not to light irradiation at 435 or 505 nm for 12 h, 24 h or 48 h. Cell viability after treatment was analysed by MTT assay [28].

2.7. MTT assay

HCT-116 p53-/- cells were seeded onto 96-well plates at density of 2 x 10^4 cells/well. Cell viability was evaluated using the MTT assay procedure, which measures the level of mitochondrial dehydrogenase activity of living cells employing the yellow 3-(4,5-dimethyl-2-thiazolyl)-2,5-diphenyl-2H-tetrazolium bromide (MTT) as substrate [29]. The absorbance was measured at 540 nm using a microplate reader (Labsystems Multiskan). Error bars represent mean ± SEM. Statistical analysis was performed as previously described [30].

2.8. Tubulin polymerization assay

Standard tubulin and tubulin ligand polymerization reactions were carried out essentially using manufacturer's instructions (tubulin polymerization assay Kit, Cytoskeleton). Briefly, in dark regime, different wells of a microtiter plate were loaded with 10 µL of buffer solution, or 10 µL of the 100 µM stock solutions of the tested reagents (taxol, **1a**, **1RR** or **1RS**). Then 90 µL of a cooled (4 °C) tubulin solution, (3.3 mg/mL) buffered at pH= 6.9 (80 mM PIPES, 0.5 mM EGTA, 2.0 mM $MgCl_2$, 1.0 mM GTP) was added to each well. Polymerization was started warming at r.t. the plate and followed by absorbance reading at 340 nm every 60 s for 3 h. In the light regimen, a similar loaded microtiter plate was kept 1 min under LED irradiation at 435 nm before starting the acquisition of the absorption data. All data were reproduced in triplicate. For each treatment, the absorption values were graphically reported *vs* time (min) as the means of the measured values.

3. RESULTS

3.1. Synthesis

Mixtures **1a** and **1b** were obtained in four synthetic steps (Scheme 1), starting from 4-nitrophenol, which was coupled with *R* or *S* glycidol, slightly modifying a previously reported procedure [31]. Despite literature data indicating that very low yields in coupling products were obtained from the reaction of *R* or *S* glycidol with diverse nitro-phenols [32], we observed that the use of catalytic amounts of KOH (in ethanol solution) favoured the formation of **2R** or **2S** in good yields with a high optical purity (Figure S1).

The reduction of **2**, as the *R* or *S* stereomer, with H_2/Pd(C) and the subsequent conversion of the amino- to the azonium-group gave rise to **4R** or **4S**, that were coupled with racemic methyl 3-hydroxy-2-(1H-pyrrol-1-*yl*)propanoate **5** [26] to give the mixtures **1a** and **1b**, respectively.

To obtain the pure diastereomers **1RS** and **1RR**, compound **4R** was coupled with the *R* or *S* stereomer of **5**. The best yields of the final coupling step were obtained by treating the reactions after 1 h from the mixture gelation. The final diastereomeric mixtures **1a** and **1b**, as well as the pure **1RR** and **1RS**, and their intermediates, were fully characterized by 1D- and 2D-NMR, HRESIMS, and UV. Furthermore, the species were analyzed on chiral HPLC (Figure S2).

3.2. UV experiments reveal the reversibility of the trans-cis conversion under different cycles of irradiation at 435 nm

UV spectra of the thermodynamically stable *trans* **1a** and **1b** were obtained in the dark, using three different solvents, MeOH, H_2O and Phoshate Buffer Solution (PBS). In all examined conditions the UV profiles of both species were similar (Figures 2A and S4). In H_2O and PBS two major broad bands with a comparable intensity, centred at 391 and 430 nm, were observed, whereas in MeOH the relative intensity of the same two bands was appreciably different. Under light exposure (400 or 435 nm), metastable *cis* isomers were obtained. Indeed, the UV profiles of **1a** and **1b** strongly changed, showing a significant decreasing of the band intensities in the range 350-460 nm, the occurrence of a new band centred at about 345 nm (Figure 2B, blue line), and a broad absorption band that extended up to 475 nm. To check the *cis*→*trans* isomerization, the UV spectra of **1a** and **1b** were sequentially collected after irradiation (Figures 2C and S3-C), and the absorbance at 390 and 345 nm was monitored over time (Figures S5-S8). In both types of experiments, the intensity of the UV band at 390 nm was almost restored in about 40 or 5 mins in the case of **1a**, and 80 or 5 mins for **1b** depending on the solvent conditions (MeOH or PBS, respectively) [33].

In the 475-550 nm range the *cis* isomers of **1a** and **1b** showed a UV absorption slightly higher than that of the corresponding *trans* (Figure 2c'). However, after irradiating the samples with green light the *cis* to *trans* conversions of **1a** and **1b** occurred faster than in darkness (Figures S9-S10).

Time-dependent UV experiments were performed also on **1RR** and **1RS** in PBS, and the resulting $t_{1/2}$s of the metastable isomers were 5.8 and 4.2 min, respectively (Figure S11).

3.3. ***^{1}H NMR spectra of samples in darkness or after irradiation at 435 nm confirm the occurrence of the 1a/b trans-cis conversion***

To gain further insights into the photo-conversion properties of **1a**, we also analyzed the progress of the *cis* to *trans* conversion by acquiring ^{1}H NMR spectra in darkness and at different times after the irradiation at 435 nm. In the dark the ^{1}H NMR spectrum of **1a** (CD_3OD, 4 mg/mL) showed in the downfield region five aromatic proton resonances at 7.70, 7.28, 7.04, 6.67, 6.32 ppm, as well as a signal at 5.62 ppm due to the proton linked to the C-α of the methyl-ester (see Supplementary data, p. 31). After light exposure (1 min, LED 435 nm) of the sample, in addition to the proton resonances attributed to the *trans* **1a**, a new set of five signals appeared in the same region of the spectrum (Figure 3). Strikingly, the intensity of the new proton signals in the spectra was inversely dependent on the sample concentration. Indeed, the ^{1}H NMR spectra, acquired on samples containing over 10 mg/mL and exposed at the same LED irradiation, did not show an appreciable amount of new proton signals. Over time, the intensities of the new signals decreased, and the ^{1}H NMR spectrum evolved towards that obtained for **1a** kept in the dark. Therefore, the transient proton signals can be related to the metastable *cis* **1a**, activated by LED light at 435 nm. The same results were obtained for **1b** (see supplementary material, p.36).

3.4. Kinetic parameters of the 1a/b and 6a/b trans→cis conversions and of the corresponding reversed isomerisations were evaluated by fast UV experiments

We also tested the occurrence of the hydrolysis of the methyl ester groups of **1a** and **1b** dissolved in PBS at r.t. During the first 2 days, neither hydrolyzed nor degraded products were observed on the HRESIMS and TLC plates. After five days from the dissolution, mass spectra corresponding to the hydrolyzed products (**6a/b**, Figure 1) were recovered (Figure S12). The UV spectra obtained after the irradiation of **6a** and **6b** in PBS showed only slight differences with those measured in darkness, thus suggesting a substantial decreasing of the life time of the corresponding metastable *cis* forms.

In order to quantify the half life time of *cis* **6a/b**, we performed kinetic studies by means of fast UV spectroscopy. Samples were made by dissolving **1a/b** in different solvents: methanol, H_2O and

PBS. **6a** and **6b** were produced as a result of the hydrolysis of **1a/b** in water-based solutions after five days from the dissolution. An exponential decay model was used to fit the kinetic data (Figure 4), to obtain the half-life times ($t_{1/2}$) for *trans* **1a**, **1b**, **6a** and **6b** to convert to their *cis* form, and for the reverse *cis* to *trans* reaction. The resulting $t_{1/2}$s are reported in Table S1. The obtained $t_{1/2}$s of *cis* **1a/b** in methanol are longer than those measured in PBS by a factor of 2-4. This is ascribed mostly to the different polarity of the two solvents, the more polar one, PBS, being characterized by a faster transition, typically associated with a lower process quantum yield [1,34]. We also notice that the two different apparatuses used to kinetically characterize the *cis*→*trans* conversions, i.e. the UV experiments based on a spectrophotometer and fast UV spectroscopy, are substantially consistent as shown by the third line in Table S1, where the $t_{1/2}$ measured for the sample of **1b** in methanol is the same, within the error range. Additionally, we observed that the measured value of the *cis* $t_{1/2}$ for the hydrolyzed products, **6a/b**, is 4-7 fold shorter than that obtained for **1a/b**, as seen in the case of the PBS (Table S1, Figures S6-S8).

3.5. The treatment with 1a, 1b, 1RR or 1RS in darkness and under irradiation affects in a different manner the viability of the HCT-116 p53-/- and A375 cells

Both **1a** and **1b** were tested by MTT assay for their ability to inhibit the HCT-116 p53-/- and A 375 cell growth at 1 and 10 μM, in the dark and under irradiation.

In darkness (Figure 5A and Figure S13A and E), at a concentration of 1 μM, both **1a** and **1b** proved to be almost ineffective on both cell lines. The viability of the HCT-116 p53-/- cells treated with **1b** at 10 μM was greater (50% at 24 h) than that of those treated with **1a** (63% at 24 h). On the contrary, at 10 μM neither **1a** nor **1b** showed any antiproliferative effect on A375 (Figure S13A and E).

Furthermore, the HCT-116 p53-/- cells were treated for 12 h with **1a** or **1b** undergoing irradiation at 435 or 505 nm. We used a pulse-program 50 ms-ON/ 1.0 min-OFF by means of an Arduino module to manage the LED plates [11]. The LED irradiation at the wavelengths used proved to be almost ineffective on the viability of the untreated cells (Figure S14).

Pulsed LED irradiation at 435 nm on HCT-116 p53-/- caused an enhancement of the antiproliferative efficiency of **1a** and **1b** at both concentrations used. Indeed, the IC_{50} of **1a** was 12.5 μM in the dark (Figure 5A) and < 1μM under irradiation (Figures 6A-B) while the IC_{50} of **1b** was 10.0 μM in the dark (Figure 5B) and in the range of 1-5 μM under irradiation (Figures 6A-C).

In order to further explore the effects of **1a** and **1b** on HCT-116 p53-/- we also used the same pulse program with LED light at 505 nm (Figure 6). Compared to the dark regimen, the viability of the cells irradiated at 505 nm and treated with **1a** or **1b** at 1 and 10 μM was only weakly affected.

In view of the photo-responsive properties of **1a**, also the pure stereomers **1RR** and **1RS** forming **1a** were investigated for their antiproliferative action on HCT-116 p53-/-, in the dark and under irradiation at 435 nm (Figure 7), following 24 h of treatment. The comparison between the resulting MTT data showed that the increase of the incubation time produced a partial loss of the antiproliferative effect of **1a (**46% *vs* 60% of viability at 1 μM and 18% *vs* 35% of viability at 10 μM) (Figures 6B and 7A). Remarkably, the mixture **1a** showed, under irradiation, a higher antiproliferative effect than each single diastereomer (Figures 6B and 7C-D) (60% cell viability of **1a** *vs* 69% for **1RR** and 78% for **1RS** at 1 μM and 35% cell viability of **1a** *vs* 65% of **1RR** and 75% of **1RS** at 10 μM)

The A375 cell line proved to be insensitive to **1a** and **1b** under irradiation, (Figure S15) also when we adopted other light regimens (besides the pulse program above mentioned we also used 50 ms ON/1.0 s OFF; 50 ms ON /500 ms OFF; and 500 ms ON/7.5 min OFF), and prolonged the incubation time from 12 to 24 h.

3.6. 1a and 1RS affect the dynamics of MT polymerization after UV irradiation

In order to evaluate the effects of **1a**, **1RR** and **1RS** on tubulin polymerization, we measured the increasing in light scattering at 350 nm over time, caused by the polymer formation from unassembled tubulin solutions. Indeed, as previously reported [35], there is almost a linear relationship between the measured turbidity generated from the tubulin solutions and the total amount of microtubules. In this assay taxol, a well known MT stabilizing agent, was used as the reference compound.

The results of the tubulin polymerization assay mainly indicated that at 10 µM **1a** and **1RS**, but not **1RR**, acted as MT destabilizing agents, hindering the tubulin polymerization [36] mostly after irradiation of the plates with LED light at 435 nm for 1 min before the data acquisition (Figures S16 and S17). Indeed, the comparison of the data on the tubulin solutions treated with 10 µM of **1a**, or **1RS**, acquired in darkness or under irradiation, showed an increasing in the $t_{1/2}$ values of the polymerization (Table 1) of about 30 and 32.2 mins, whereas 10 µM of **1RR** did not significantly affect the $t_{1/2}$ of tubulin.

compounds 10 µM	**$t_{1/2}$ after irradiation (min)**	**$t_{1/2}$ in the dark (min)**
buffer	61.0±0.1	
taxol	10.2 ±0.4	
1a	97.0±1.0	66.5±0.2
1RR	66.9±0.5	62.3±0.2
1RS	104.0±1.0	71.8±0.5

Table 1. The $t_{1/2}$ of the tubulin polymerization (≈66 µM) calculated from the fitted curves in the presence of 10 µM of **1a**, **1RR** or **1RS** in the dark and under LED irradiation at 435 nm.

4. Discussion

In this study some chiral benzodiazo *N*-substituted pyrrole derivatives as potential photo-activable MTAs were synthesized and their biophysical properties were explored by means of UV, fast UV, NMR, MTT and tubulin polymerization assay. All the collected UV and NMR data suggested that irradiation of the samples at 435 nm induced the conversion of the thermodynamically stable *trans* **1a** and **1b** to the corresponding metastable *cis* forms, and that a *cis* to *trans* reversion occurred in darkness. Indeed, after LED light irradiation, the UV profiles significantly changed and then evolved over time to become those obtained in the dark. Correspondingly, the comparison between ^{1}H NMR acquired in the dark and after LED exposure showed that the irradiation of the samples caused the occurrence of new and transient proton signals, attributable to the presence of the metastable *cis* isomers in the solution. The kinetics of the **1a/b** *cis-trans* conversions was evaluated by both UV and fast UV spectroscopy. The obtained data suggested that, in methanol, but not in PBS, the chirality of the substituent at the oxygen atom of the benzene ring significantly affects the half lives of the metastable *cis* forms (Figures S5-S8 and Table S1)**.**

The occurrence of the hydrolysis of the methyl ester group in **1a/b** in PBS at pH= 7.4 was also evaluated. The hydrolysis of **1a/b** in **6a/b** also caused a significant decreasing of the half lives of the metastable *cis* isomers, evaluated by means of UV spectroscopy. Our data are consistent with the literature [37-38]. In particular, it appears that the solvation of diazocompounds by polar solvents positively affects the rate of *cis/trans* isomerization. Accordingly, in PBS the free carboxyl group in **6a/b** should promote the solute-solvent interactions, thus producing a decreasing in the half-lives of *cis* **6a/b** with respect to **1a/b.**

In order to explore the antiproliferative activity of **1a/b** and **1RR/RS** on cancer cell lines, a MTT assay on HCT 116 p53 -/- and A375 was performed, both in the dark and under LED irradiation at 435 nm. The overall results showed that only HCT 116 p53-/- was responsive to the treatments.

It is noteworthy that both CA4 and the PSTs inhibit the A375 cell proliferation [11,39]. This finding could be ascribed to a greater structural similarity between CA4 and the previously reported PSTs than between CA4 and the herein described molecules. Considering that:

i) CA4 potently inhibits the A375 cell growth with an IC_{50} in the range of nanomolar concentrations;

ii) A375 and melanoma cells, in general, are resistant to the induction of apoptosis when exposed to chemotherapeutic agents via the activation of different protective mechanisms [40]; and

iii) the *in vitro* polymerization experiments showed an impact of **1a/b** on tubulin, but the effect on the $t_{1/2}$ of tubulin is moderate (Table 1)

we suggest that CA4 and **1a/b** could have a different mode of action. This hypothesis could be supported also by the results obtained by Borowiak et al. [11]. Indeed, although PST-1 shares an almost complete structural similarity with CA4, it inhibits cancer cell growth more significantly than *in vitro* tubulin polymerization.

On the HCT 116 p53-/- cell line the *cis* stereomers forming **1a** and **1b** exhibited a greater antiproliferative effect than the corresponding thermodynamically stable *trans.* Furthermore, the photo-responsive antiproliferative profile of **1a** appeared more promising than that of **1b.**

On irradiating the HCT 116 p53 -/- cells with green light (505 nm) an *in vitro* reversion of the *cis* **1a** toxic effect only partially occurred. The UV spectra of **1a** and **1b** irradiated with LED at 435 nm or 505 nm also showed that the *trans* to *cis* conversion was efficiently induced only by LED at 435 nm (Figures 2, S4 and the ^{1}H NMR spectra after irradiation at 505 nm in the SI), while the green light promoted, in part, the *cis* to *trans* conversion (Figures S9 and S10). In addition, the inability of the green light to promote this reversion has also been observed for some PSTs by Borowiak et al. [11] and should depend on the small difference in the absorption band between the *trans/cis* isomers.

The time-dependent UV experiments in PBS revealed that the $t_{1/2}$s of *cis* **1RR** and *cis* **1RS**, the pure stereomers forming **1a**, were slightly different (5.8 and 4.2 min, respectively, Figure S11) whereas the average of the two values corresponded to that of **1a** (Figures S5 and S6). On prolonging the incubation time from 12 to 24 h a partial loss of the toxic effect of **1a** on HCT-116 p53-/- was also observed both in the dark and under irradiation at 435 nm (Figures 5A, 6 and 7). This occurrence has previously been described and could be attributed to the reduction of the diazo-compounds by intracellular glutathione [13].

Remarkably, under irradiation, the antiproliferative effect of **1a** on HCT 116 p53-/- was greater than that of each single diastereomer (Figure 7B-C-D). Similar phenomena have already been observed [41,42]; nevertheless, the apparent synergic behaviour of **1RR** and **1RS** is peculiar, since it was amplified upon photo-activation (Figure 7A-B).

Finally, the $t_{1/2}$ values obtained from the tubulin polymerization curves showed that the ability of **1a**, **1RR** and **1RS** to interfere with the MT dynamics was activated by LED irradiation. Strikingly, the chirality *S* of the substituent on the pyrrole portion in **1RS** appeared essential to inhibit the tubulin polymerization.

Despite the fact that more in-depth studies should be performed to clarify the reasons for these *in vitro* properties, the described benzodiazo *N*-substituted pyrrole derivatives represent leads for the discovery of a new class of photo-activable compounds useful for the local control of cancer cell growth. Indeed, **1a** contains four functional groups, that can be, in the future, easily employed to produce a large number of **1a** analogues, properly designed to improve both the antiproliferative activity and the glutathione resistance [1-3, 43-44].

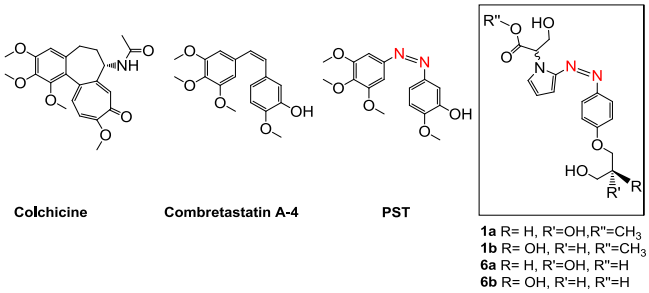

Figure 1. Natural ligands of MTs and AzB analogues.

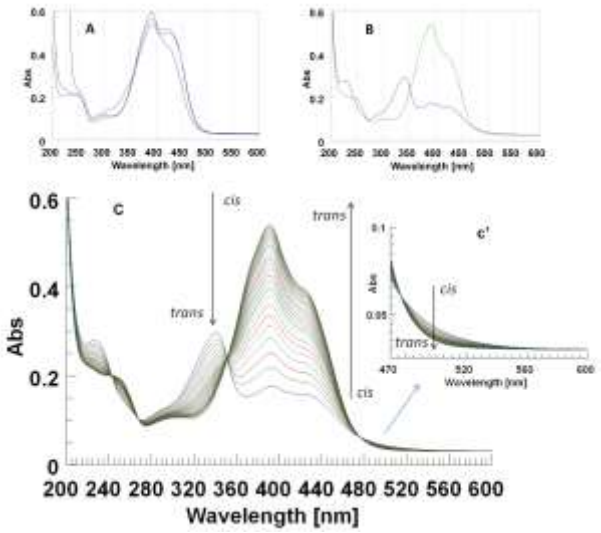

Figure 2. A. The UV spectra of **1a** in MeOH (black), PBS (blue) and H_2O (violet). **B**. The UV spectra of **1a** in MeOH before (green) and after (blue) irradiation at 435 nm. **C**. The time-dependent UV spectra of **1a** (2 min) after irradiation at 400 nm in MeOH. The time gap between the two consecutive spectra was 2 mins. **c'**. The enlargement of the spectra was in the range 475-550 nm.

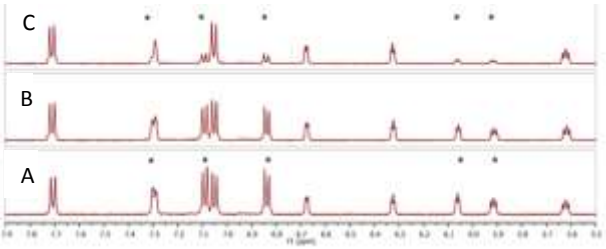

Figure 3. The ^{1}H NMR spectra (CD_3OD) of **1a** (7.9-5.5 ppm), sequentially acquired after 3 mins (**A**), 10 mins (**B**), and 25 mins (**C**) from the irradiation at 435 nm. The transient resonances indicated by asterisks were produced by the protons of the metastable *cis* **1a**.

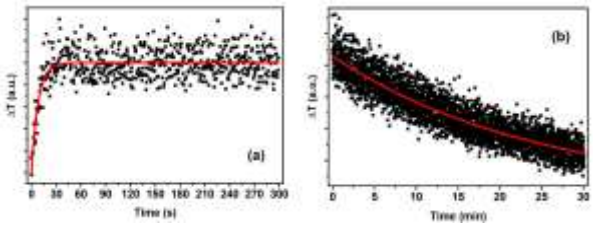

Figure 4. An example of the 404-nm probe transmitted intensity changes: passing through **1b** in methanol solution as a function of time; (**a**) the *trans* to *cis* conversion [when the laser is switched on and the sample is being irradiated with 10 mW, 435 nm laser beam], and (**b**) the *cis* to *trans* conversion [in the dark].

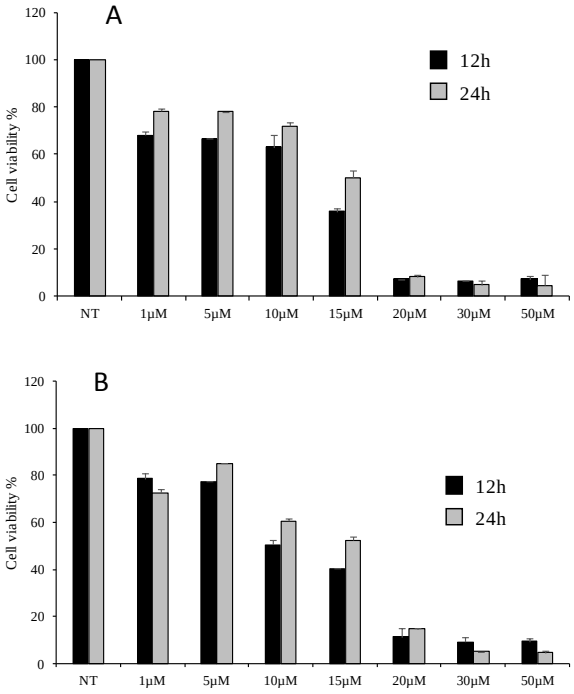

Figure 5. Dose-response experiments on HCT-116 p53-/- treated in darkness with **1a** (A) and **1b** (B) at different incubation times (12 and 24 h). The data are presented as a percentage (mean ± SEM) of the viability of the untreated control cells (NT). The calculated IC_{50}s at 12 h are 12.5 and 10 µM, for **1a** and **1b,** respectively.

.

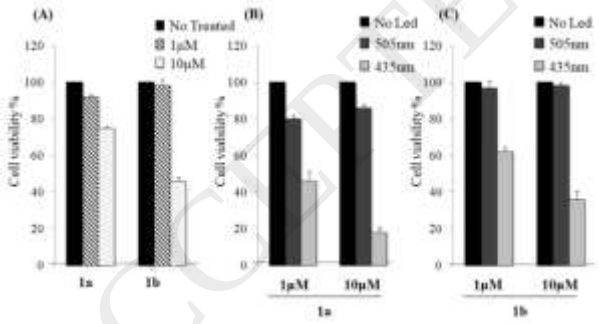

Figure 6. The HCT-116 p53-/- cell viability in the MTT assay conducted in different conditions. (**A**) Cells treated for 12 h with **1a** or **1b**, in the dark. The results are presented as a percentage (mean ± SEM) of the untreated control cells. (**B** and **C**) Cells treated with **1a** or **1b** and irradiated for 12 h with LED light at 505 or 435 nm (12 h, 50 ms-ON/ 1.0 min-OFF). The results are presented as a percentage (mean ± SEM) of the control cells treated in the dark with **1a** or **1b**.

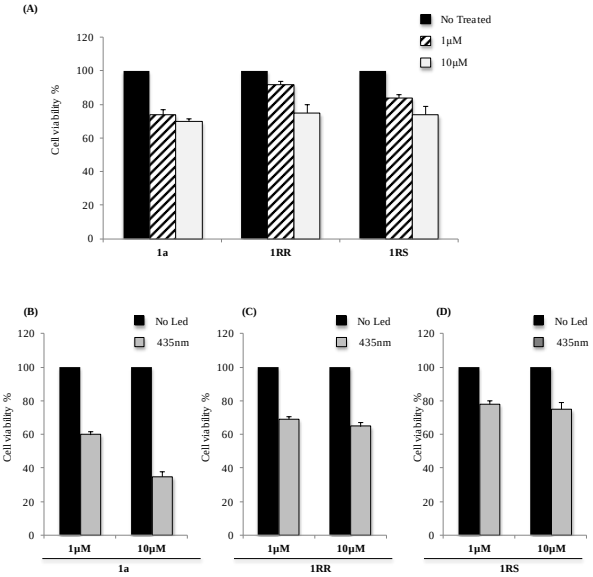

Figure 7. The HCT-116 p53-/- cell viability in the MTT assay conducted in different conditions. (**A**) Cells treated for 24 h with **1a**, **1RR** or **1RS** in the dark. The results are presented as a percentage (mean ± SEM) of the untreated control cells. (**B**, **C** and **D**) Cells treated with **1a**, **1RR** and **1RS** respectively and irradiated for 24 h with LED at 435 nm (12 h, 50 ms-ON/ 1.0 min-OFF). The results are presented as a percentage (mean ± SEM) of the control cells treated in the dark.

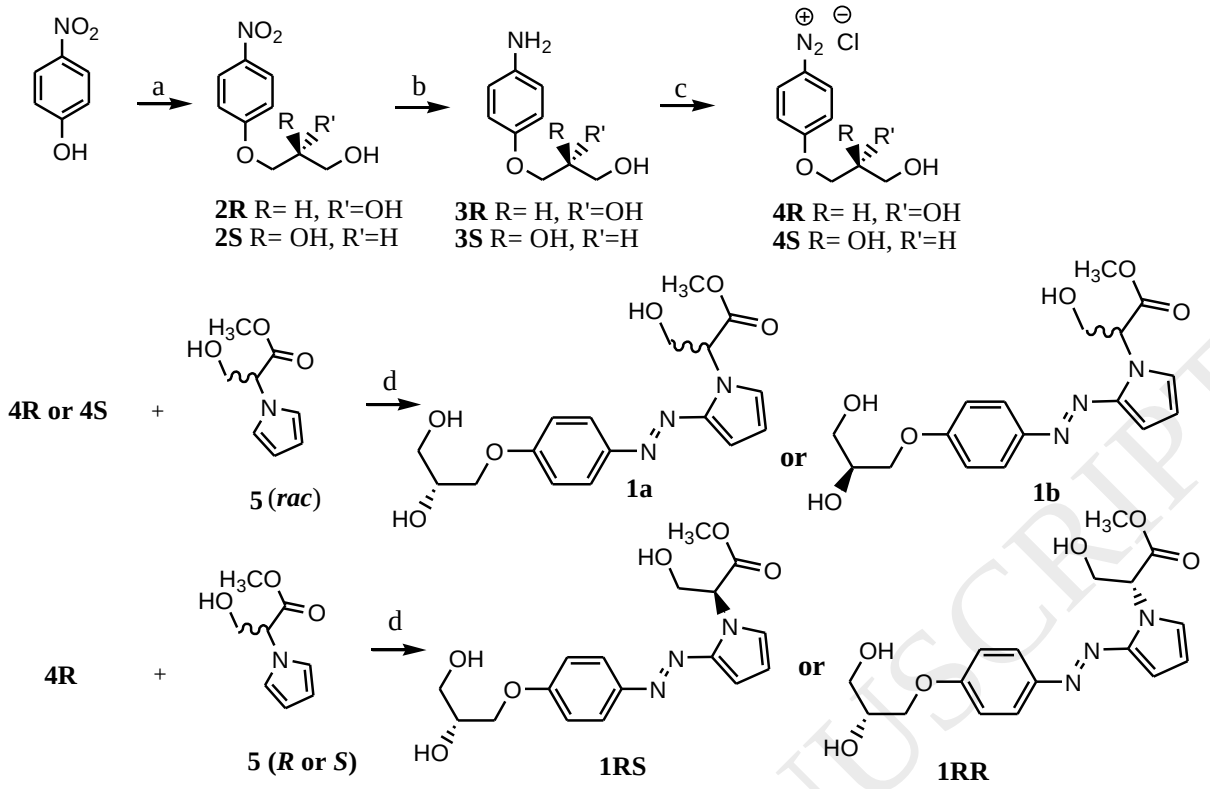

Scheme 1. Preparation of compounds **1a**, **1b**, **1RS**, and **1RR.** Reagents and conditions: a) catalytic KOH, dry toluene, 30 mins under reflux, then addition of *R* or *S* glycidol at r.t., and heating at 90 °C for 24h; b) Pd/C, H_2 (P= 400 psi) in EtOH, 2 h, r.t. c) fluoroboric acid (water solution, 48%), EtOH,- 15 °C, then isoamyl nitrite, r.t., 12 h; d) acetic acid, sodium acetate 1 h, r.t.

Conflicts of interest: There are no conflicts to declare**.**

Acknowledgements
This research was funded by Regione Campania under POR Campania FESR2007-2013 −O.O. 2.1 (FarmaBioNet). The authors are grateful to "Istituto Tecnico Industriale Statale Francesco Giordani of Caserta" (I.T.I.S. Giordani) for their technical assistance on the LED System construction**.**

References

[1] K. Hüll, J. Morstein, D. Trauner, In vivo photopharmacology, Chem. Rev. 118 (2018) 10710−10747. doi: 10.1021/acs.chemrev.8b00037.
[2] W.A. Velema, W. Szymanski, B.L. Feringa, Photopharmacology: beyond proof of principle, J. Am. Chem. Soc. 136 (2014) 2178−2191. doi: 10.1021/ja413063e.
[3] J. Broichhagen, J.A. Frank, D. Trauner, A roadmap to success in photopharmacology, Acc. Chem. Res. 48 (2015) 1947−1960. doi: 10.1021/acs.accounts.5b00129.
[4] J. García-Amorós, D. Velasco, Recent advances towards azobenzene-based light driven real-time information-transmitting materials, Beilstein J. Org. Chem. 8 (2012) 1003–1017. doi: 10.3762/bjoc.8.113.
[5] M. Dong, A. Babalhavaeji, S. Samanta, A.A. Beharry, G.A. Woolley, Red-shifting azobenzene photoswitches for in vivo use, Acc. Chem. Res. 48 (2015) 2662−2670. doi: 10.1021/acs.accounts.5b00270.
[6] E.C. Carrolla, S. Berlin, J. Levitz, M.A. Kienzler, Z. Yuan, D. Madsen, D.S. Larsen, E.Y. Isacoff, Two-photon brightness of azobenzene photoswitches designed for glutamate receptor optogenetics, PNAS 112 (2015) E776–E785. doi: 10.1073/pnas.1416942112.
[7] M.A. Kienzler, A. Reiner, E. Trautman, S. Yoo, D. Trauner, E.Y. Isacoff, A red-shifted, fast-relaxing azobenzene photoswitch for visible light control of an ionotropic glutamate receptor, J. Am. Chem. Soc. 135 (2013) 17683−17686. doi: 10.1021/ja408104w.
[8] A. Bergen, S. Rudiuk, M. Morel, T. Le Saux, H. Ihmels, D. Baigl, Photodependent melting of unmodified dna using a photosensitive intercalator: a new and generic tool for photoreversible assembly of dna nanostructures at constant temperature, Nano Lett. 16 (2016) 773−780. doi: 10.1021/acs.nanolett.5b04762.
[9] O. Sadovski, A.A. Beharry, F. Zhang, G.A. Woolley, Spectral tuning of azobenzene photoswitches for biological applications, Angew. Chem. Int. Ed. 48 (2009) 1484 –1486. doi: 10.1002/anie.200805013.
[10] S. Pipolo, E. Benassi, S. Corni, Structural properties of azobenzene self-assembled monolayers by atomistic simulations, Langmuir 29 (2013) 10505−10512. doi: 10.1021/la404922f.
[11] M. Borowiak, W. Nahaboo, M. Reynders, K. Nekolla, P. Jalinot, J. Hasserodt, M. Rehberg, M. Delattre, S. Zahler, A. Vollmar, D. Trauner, O. Thorn-Seshold, Photoswitchable inhibitors of microtubule dynamics optically control mitosis and cell death, Cell 162 (2015) 403–411. doi: 10.1016/j.cell.2015.06.049.
[12] A.J. Engdahl, E.A. Torres, S.E. Lock, T.B. Engdahl, P.S. Mertz, C.N. Streu, Synthesis, characterization, and bioactivity of the photoisomerizable tubulin polymerization inhibitor azo-Combretastatin A4, Org. Lett. 17 (2015) 4546−4549. doi: 10.1021/acs.orglett.5b02262.
[13] J.E. Sheldon, M.M. Dcona, C.E. Lyons, J.C. Hackett, M.C.T. Hartman, Photoswitchable anticancer activity via trans–cis isomerization of a combretastatin A-4 analog, Org. Biomol. Chem. 14 (2016) 40−49. doi: 10.1039/c5ob02005k.
[14] A.L. Parker, M. Kavallaris, J.A. McCarroll, Microtubules and their role in cellular stress in cancer, Front. Oncol. 18 (2014) Article 153. doi: 10.3389/fonc.2014.00153.

[15] S.X. Zhang, J.Feng, S.C. Kuo, A. Brossi, E. Hamel, A. Tropsha, K.-H. Lee, Antitumor Agents. 199. Three-dimensional quantitative structure-activity relationship study of the colchicine binding site ligands using comparative molecular field analysis, J. Med. Chem. 43 (2000) 164−175. doi: 10.1021/jm990333a.
[16] Y. Shen, L. Wu, L. Qiu, Water-soluble combretastatin a4 phosphate orally delivered via composite nanoparticles with improved inhibition effect toward s180 tumors, J. Pharm. Sci. 106 (2017) 3076-3083. doi: 10.1016/j.xphs.2017.05.031.
[17] P. Zhou, Y. Liu, L. Zhou, K. Zhu, K. Feng, H. Zhang, Y. Liang, H. Jiang, C. Luo, M. Liu, Y. Wang, Potent antitumor activities and structure basis of the chiral β‑lactam bridged analogue of combretastatin a-4 binding to tubulin, J. Med. Chem. 59 (2016) 10329–10334. doi: 10.1021/acs.jmedchem.6b01268.
[18] S.K. Rastogi Z. Zhao, S.L. Barrett, S.D. Shelton, M. Zafferani, H.E. Anderson, M.O. Blumenthal, L.R. Jones, L. Wang, X. Li, C.N. Streu, L. Du, W.J. Brittain, Photoresponsive azo-combretastatin A-4 analogues, Eur. J. Med. Chem. 143 (2018) 1−7. doi: 10.1016/j.ejmech.2017.11.012.
[19] Z.S. Seddigi, M.S. Malik, A.P. Saraswati, S.A. Ahmed, A.O. Babalghith, H.A. Lamfon A. Kamal, Recent advances in combretastatin based derivatives and prodrugs as antimitotic agents, Med. Chem. Commun. 8 (2017) 1592–1603. doi: 10.1039/c7md00227k.
[20] S. Zheng, Q. Zhong, M. Mottamal, Q. Zhang, C. Zhang, E. Lemelle, H. McFerrin, G. Wang, Design, synthesis, and biological evaluation of novel pyridine-bridged analogues of combretastatin-A4 as Anticancer Agents, J. Med. Chem. 57 (2014) 3369−3381. doi: 10.1021/jm500002k.
[21] D. Tarade, D. Ma, C. Pignanelli, F. Mansour, D. Simard, S. van den Berg, J. Gauld, J. McNulty, S. Pandey, Structurally simplified biphenyl combretastatin A4 derivatives retain in vitro anti-cancer activity dependent on mitotic arrest, PLoS ONE 12 (2017) e0171806. doi: 10.1371/journal.pone.0171806.
[22] J. Garcia-Amorós, M.C.R. Castro, P. Coelho, M.M.M. Raposo, D. Velasco, New heterocyclic systems to afford microsecond green-light isomerisable azo dyes and their use as fast molecular photochromic switches, Chem. Comm. 49 (2013) 11427-11429. doi: 10.1039/c3cc46736h.
[23] T.T. Yin, Z.X. Zhao, H.X. Zhang, A theoretical study on the thermal cis–trans isomerization of azoheteroarene photoswitches, New J. Chem. 41 (2017) 1659−1669. doi: 10.1039/c6nj03095e
[24] J. Calbo, C.E. Weston, A.J.P. White, H.S. Rzepa, J. Contreras-García, M.J. Fuchter, Tuning azoheteroarene photoswitch performance through heteroaryl design, J. Am. Chem. Soc. 139 (2017) 1261−1274. doi: 10.1021/jacs.6b11626.
[25] A. Vogel, V. Venugopalan, Mechanisms of pulsed laser ablation of biological tissues, Chem. Rev. 103 (2003) 577-644. doi: 10.1021/cr010379n.
[26] B.S. Gourlay, P.P. Molesworth, J.H. Ryan, J.A. Smith, A new and high yielding synthesis of unstable pyrroles via a modified Clauson-Kaas reaction, Tetrahedron Lett. 47 (2006) 799−801. doi: 10.1016/j.tetlet.2005.11.104.
[27] A. Russo, S. Maiolino, V. Pagliara, F. Ungaro, F. Tatangelo, A. Leone, G. Scalia, A. Budillon, F. Quaglia, G. Russo, Enhancement of 5-FU sensitivity by the proapoptotic rpL3 gene in p53 null colon cancer cells through combined polymer nanoparticles, Oncotarget 7 (2016) 79670-79687. doi: 10.18632/oncotarget.13216.
[28] D. De Filippis, A. Russo, D. De Stefano, M. Cipriano, D. Esposito, G. Grassia, R. Carnuccio, G. Russo, T. Iuvone, Palmitoylethanolamide inhibits rMCP-5 expression by regulating MITF activation in rat chronic granulomatous inflammation, Eur. J. Pharmacol. 725 (2014) 64−69. doi: 10.1016/j.ejphar.2013.12.021.

[29] A. Russo, A. Saide, R. Cagliani, M. Cantile, G. Botti, G. Russo, rpL3 promotes the apoptosis of p53 mutated lung cancer cells by down-regulating CBS and NFκB upon 5-FU treatment, Sci. Rep. 6 (2016) 38369. doi: 10.1038/srep38369.
[30] A. Russo, A. Saide, S. Smaldone, R. Faraonio, G. Russo, Role of uL3 in multidrug resistance in p53-mutated lung cancer cells, Int. J. Mol. Sci. 18 (2017) E547. doi: 10.3390/ijms18030547.
[31] J. Xia, E.B. Stephens, M. Mason, J.W. Miley, L.J. Starks, Polymeric Bis-acetoacetanilide azo colorants, EP 46 (2013)2 661 168-2 663 174.
[32] Z.A. Bredikhina, A.V. Kurenkov, O.A. Antonovich, A.V. Pashagin, A.A. Bredikhin, A rare case of facial selectivity inversion for Sharpless asymmetric dihydroxylation in a series of structurally homogeneous substrates: synthesis of non-racemic 3-(nitrophenoxy)-propane-1,2-diols, Tetrahedron: Asymmetry 25 (2014) 1015-1021. doi: 10.1016/j.tetasy.2014.05.008.
[33] C.E. Weston, R.D. Richardson, P.R. Haycock, A.J.P. White, M.J. Fuchter, Arylazopyrazoles: azoheteroarene photoswitches offering quantitative isomerization and long thermal half-lives, J. Am. Chem. Soc. 136 (2014) 11878-11881. doi: 10.1021/ja505444d.
[34] P. Bortolus, S. Monti, Cis-Trans photoisomerization of azobenzene. solvent and triplet donor effects, J. Phys. Chem. 83 (1979) 648-652. doi: 10.1021/j100469a002.
[35] J.M. Batista, A.N.L. Batista, D. Rinaldo, W. Vilegas, D.L. Ambrósio, R.M.B. Cicarelli, V.S. Bolzani, M.J. Kato, L.A. Nafie, S.N. López, M. Furlan, Absolute configuration and selective trypanocidal activity of gaudichaudianic acid enantiomers, J. Nat. Prod. 74 (2011) 1154-1160. doi: 10.1021/np200085h.
[36] C. Dumontet, M.A. Jordan, Microtubule-binding agents: a dynamic field of cancer therapeutics, Nat. Rev. Drug Discov. 9 (2010) 790–803. doi: 10.1038/nrd3253.
[37] N.J. Dunn, W.H. Humphries, A.R. Offenbacher, T.L. King, J.A. Gray, pH-dependent cis → trans isomerization rates for azobenzene dyes in aqueous solution, J. Phys. Chem. A 113 (2009), 13144-13151. doi: 10.1021/jp903102u
[38] M. Kojima, S. Nebashi, K. Ogawa, N. Kurita, Effect of solvent on cis-to-trans isomerization of 4-hydroxyazobenzene aggregated through intermolecular hydrogen bonds, J. Phys. Org. Chem. 18 (2005) 994-1000. doi: 10.1002/poc.944.
[39] S. Madhavi, R. Sreenivasulu, J.P. Yazala, R.R. Raju, Synthesis of chalcone incorporated quinazoline derivatives as anticancer agents, Saudi Pharm. J. 25 (2017), 275–279. doi: 10.1016/j.jsps.2016.06.005.
[40] D. Grossman, D.C. Altieri, Drug resistance in melanoma: Mechanisms, apoptosis, and new potential therapeutic targets, Cancer Metastasis Rev 20 (2001), 3-11. doi: 10.1023/A:1013123532723.
[41] C. Bonfils, N. Bec, B. Lacroix, M.-C. Harricane, C. Larroque, Kinetic analysis of tubulin assembly in the presence of the microtubule-associated protein TOGp, J. Biol. Chem. 282 (2007) 5570–5581. doi: 10.1074/jbc.M605641200.
[42] Z.H. Tang, Y.B. Liu, S.G. Ma, L. Li, Y. Li, J.D. Jiang, J. Qu, S.S. Yu, Antiviral spirotriscoumarins a and b: two pairs of oligomeric coumarin enantiomers with a spirodienone–sesquiterpene skeleton from *Toddalia asiatica*, Org. Lett. 18 (2016) 5146-5149. doi: 10.1021/acs.orglett.6b02572.
[43] S. Samanta, T.M. McCormick, S.K. Schmidt, D.S. Seferos, G.A. Woolley, Robust visible light photoswitching with ortho-thiol substituted azobenzenes, Chem. Comm. 49 (2013) 10314-10316. doi: 10.1039/c3cc46045b.
[44] C. Knie, M. Utecht, F. Zhao, H. Kulla, S. Kovalenko, A.M. Brouwer, P. Saalfrank, S.Hecht, D. Bléger, ortho-Fluoroazobenzenes: visible light switches with very long-lived z isomers, Chem. Eur. J. 20 (2014) 16492-16501. doi: 10.1002/chem.201404649.